

Intrinsic two-dimensional multiferroicity in $CrNCl_2$ monolayer

Wei Shen(沈威), Yuanhui Pan(潘远辉), Shengnan Shen(申胜男), Hui Li(李辉), Siyuan Nie(聂思媛), and Jie Mei(梅杰)

Citation: Chin. Phys. B, 2021, 30 (**11**): 117503. DOI: 10.1088/1674-1056/ac0787
Journal homepage: http://cpb.iphy.ac.cn; http://iopscience.iop.org/cpb

What follows is a list of articles you may be interested in

Strain drived band aligment transition of the ferromagnetic VS_2/C_3N van der Waals heterostructure

Jimin Shang(商继敏), Shuai Qiao(乔帅), Jingzhi Fang(房景治), Hongyu Wen(文宏玉), and Zhongming Wei(魏钟鸣)

Chin. Phys. B, 2021, 30 (**9**): 097507. DOI: 10.1088/1674-1056/ac0cd1

Vertical WS_2 spin valve with Ohmic property based on Fe_3GeTe_2 electrodes

Ce Hu(胡策), Faguang Yan(闫法光), Yucai Li(李予才), and Kaiyou Wang(王开友)

Chin. Phys. B, 2021, 30 (**9**): 097505. DOI: 10.1088/1674-1056/ac078b

Gate-controlled magnetic transitions in Fe_3GeTe_2 with lithium ion conducting glass substrate

Guangyi Chen(陈光毅), Yu Zhang(张玉), Shaomian Qi(齐少勉), and Jian-Hao Chen(陈剑豪)

Chin. Phys. B, 2021, 30 (**9**): 097504. DOI: 10.1088/1674-1056/ac1338

Magnetic dynamics of two-dimensional itinerant ferromagnet Fe_3GeTe_2

Lijun Ni(倪丽君), Zhendong Chen(陈振东), Wei Li(李威), Xianyang Lu(陆显扬), Yu Yan(严羽), Longlong Zhang(张龙龙), Chunjie Yan(晏春杰), Yang Chen(陈阳), Yaoyu Gu(顾耀玉), Yao Li(黎遥), Rong Zhang(张荣), Ya Zhai(翟亚), Ronghua Liu(刘荣华), Yi Yang(杨燚), and Yongbing Xu(徐永兵)

Chin. Phys. B, 2021, 30 (**9**): 097501. DOI: 10.1088/1674-1056/ac0e25

Magnon bands in twisted bilayer honeycomb quantum magnets

Xingchuan Zhu(朱兴川), Huaiming Guo(郭怀明), and Shiping Feng(冯世平)

Chin. Phys. B, 2021, 30 (**7**): 077505. DOI: 10.1088/1674-1056/abeee5

Intrinsic two-dimensional multiferroicity in $CrNCl_2$ monolayer*

Wei Shen(沈威)[1,2,3,†], Yuanhui Pan(潘远辉)[1,3,†], Shengnan Shen(申胜男)[1,2,‡], Hui Li(李辉)[1,2,§], Siyuan Nie(聂思媛)[1], and Jie Mei(梅杰)[4]

[1] *School of Power and Mechanical Engineering, Wuhan University, Wuhan* 430072, *China*
[2] *Research Institute of Wuhan University in Shenzhen, Shenzhen* 518057, *China*
[3] *Department of Quantum and Energy Materials, International Iberian Nanotechnology Laboratory, Braga* 4715-330, *Portugal*
[4] *School of Logistic Engineering, Wuhan University of Technology, Wuhan* 430070, *China*

(Received 2 February 2021; revised manuscript received 24 March 2021; accepted manuscript online 3 June 2021)

Two-dimensional multiferroics, which simultaneously possess ferroelectricity and magnetism in a single phase, are well-known to possess great potential applications in nanoscale memories and spintronics. On the basis of first-principles calculations, a $CrNCl_2$ monolayer is reported as an intrinsic multiferroic. The $CrNCl_2$ has an antiferromagnetic ground state, with a Néel temperature of about 88 K, and it exhibits an in-plane spontaneous polarization of 200 pC/m. The magnetic moments of $CrNCl_2$ mainly come from the d_{xy} orbital of the Cr cation, but the plane of the d_{xy} orbital is perpendicular to the direction of the ferroelectric polarization, which hardly suppresses the occurrence of ferroelectricity. Therefore, the multiferroic exits in the $CrNCl_2$. In addition, like $CrNCl_2$, the $CrNBr_2$ is an intrinsic multiferroic with antiferromagnetic-ferroelectric ground state while $CrNI_2$ is an intrinsic multiferroic with ferromagnetic-ferroelectric ground state. These findings enrich the multiferroics in the two-dimensional system and enable a wide range of applications in nanoscale devices.

Keywords: two-dimensional multiferroic $CrNCl_2$ monolayer magnetism ferroelectricity

PACS: 75.85.+t, 77.55.Nv, 82.45.Mp, 63.20.dk **DOI:** 10.1088/1674-1056/ac0787

1. Introduction

Nanoscale spin-based electronics (or spintronics),[1,2] using the spins of electrons for future generation of information storage, transmission and processing with the promising advantages of high storage density, high integration density, low energy consumption and high device operation speed,[3,4] are drawing more and more research interests these years. Unfortunately, most of those explored two-dimensional (2D) materials, such as graphene,[5] h-BN[6] and phosphorene,[7] possess none or weak intrinsic ferromagnetic (FM) ordering, which block their direct applications in spintronics. It is reported that magnetism in 2D materials can be induced by the process of adsorption,[8] doping,[9] defect engineering[10] and chemical functionalization,[11] the artificially induced magnetism, however, until now it has been observed to be rather weak.[12,13] For 2D ferromagnetic materials used in spintronic devices, the coexistence of a large spin polarization and a high enough Curie temperature is of great interest and importance.[4,14,15] So far, a few 2D materials have been reported to be potential in spintronic devices, such as $Cr_2Ge_2Te_6$.[14] MnN,[16] CoH_2,[17] and Cr_3Te_4,[18] and there are more 2D materials to be discovered. Analogous to ferromagnetism, ferroelectric (FE) materials are those with spontaneous electric polarization which is switchable by an external electric field.[19] FE materials have promising potentials in applications of non-volatile memories,[20,21] fieldeffect transistors,[22,23] sensors and photonics devices.[24–26] Meanwhile, ultrathin FE films are clearly needed in today's industrial applications, in a necessary attempt to improve the integrity and energy efficiency.[27–30] However, when a three-dimensional FE perovskite oxide is thinned down to a critical thickness of around several to tens of nanometers, its spontaneous polarization usually disappears, because of the reduced long-range Coulomb coupling, depolarizing electrostatic field, the effects of surface energy and electron screening.[27,29,30] Up to date, a few 2D materials have been revealed or predicted to exhibit stable ferroelectricity, including 1T-MoS_2,[31] SnTe[32] and $CuInP_2S_6$.[33] Still, plenty of 2D ferroelectrics are out there waiting to be explored.

Multiferroics, which simultaneously exhibit ferroelectricity and magnetism in a single phase, have been intriguing intensive interests due to their novel physics and promising applications in memories and spintronics.[34–36] There are two kinds of multiferroics that have been reported. In type-I multiferroics, the FE and FM orders originate from different sources

*Project supported by the National Key R&D Program of China (Grant No. 2019YFB1704600), the International Cooperation Research Project of Shenzhen (Grant No. GJHZ20180413182004161), the Hubei Provincial Natural Science Foundation of China (Grant No. 2020CFA032), the National Natural Science Foundation of China (Grant No. 51805395), and the China Scholarship Council (Grant No. 201906270142).

†Wei Shen and Yuanhui Pan contributed equally to this work.
‡Corresponding author. E-mail: shen_shengnan@whu.edu.cn
§Corresponding author. E-mail: li_hui@whu.edu.cn

© 2021 Chinese Physical Society and IOP Publishing Ltd

and meanwhile they usually couple weakly. However, the ferroelectricity is resulted from the FM order which breaks the centrosymmetry in type-Ⅱ multiferroics. In type-Ⅱ multiferroics, the magnetoelectric coupling is usually strong, and yet their FE orders are often very weak and the Curie temperature is rather low.[37,38] Therefore, to reach ideal multiferroics, one direction is to merge their strength together in one material. Although with many promising and appealing applications, only a few 2D multiferroic candidates have been reported so far, such as magnetic-FE $Hf_2VC_2F_2$,[39] FM-FE electron-doped $CrBr_3$ monolayer,[40] $VOCl_2$ monolayer[41,42] and Fe_2O_3 monolayer.[43] However, scientific evidences of intrinsic multiferroicity in 2D materials without artificial treatments like surface treatment and doping are rather rare so far. In this work, based upon the first-principles calculations, we propose an intrinsic multiferroic, $CrNCl_2$ monolayer.

2. Method

All of the calculations are carried out based on the density functional theory (DFT) as implemented in the Vienna *ab initio* simulation package (VASP)[44,45] within the projector augmented-wave method.[46] General gradient approximation in the Perdew–Burke–Ernzerhof[47] expression is chosen as the exchangecorrelation functional. The plane-wave cutoff energy is set to be 600 eV. A vacuum space of 15 Å is added between each monolayer to avoid the spurious interaction between each layer and its periodic replicate. The k-points grids of $12\times12\times1$ and $6\times6\times1$ under the Monkhorst–Pack k-points scheme[48] are employed to sample the Brillouin zone for the unit cell and $2\times2\times1$ supercell, respectively. The convergence criteria are set to be 0.005 eV/Å for the force during the structural relaxation and 10^{-6} eV for energy. The convergence of the setting has been tested and verified. First-principles molecular dynamics (MD) simulations are carried out using the canonical (NVT) ensemble[49] with a time step of 1.0 fs for 10 ps. The polarization calculation is performed by the Berry phase method,[50] in which both the electronic and ionic contributions are taken into account. The minimum energy paths of FE transitions are deduced by the climbing image nudged elastic band (CINEB) method,[51] which is based upon the interatomic forces and total energies calculated from the DFT simulations. The Dudarev implementation[52] is used with an on-site Coulomb interaction $U_{\rm eff}=U-J$ applied to the 3d orbitals. A detailed calculation on different $U_{\rm eff}$ is listed in Table S2 in the supporting information.

3. Results and discussion

3.1. Geometry and stability

Firstly, the energetic ground-state of $CrNCl_2$ monolayer is searched. Inspired by the newly reported $VOCl_2$,[41,42] the $CrNCl_2$ monolayer is designed with a similar structure, so are $CrNBr_2$ and $CrNI_2$. Through geometry optimization without any symmetry constraints, the stable $CrNCl_2$ monolayer structure is found, and computational details are shown in the supporting information. In the following study, the electronic, magnetic and ferroelectric properties of the $CrNCl_2$ monolayer will be focused.

The optimized atomic structure of $CrNCl_2$ monolayer is illustrated in Fig. 1. The black dashed rectangle in Fig. 1(a) denotes the structural unit cell, and it exhibits *Pmm*2 symmetry. As depicted in Fig. 1(b), each Cr atom connects to two N atoms and four halogen atoms, showing an octahedral framework. Like $VOCl_2$ proposed by Ai *et al.*,[41] there is no central inversion symmetry in the $CrNCl_2$ monolayer. The Cr atom moves towards one of the bridging N atoms along the basis vector a (as the z-direction), and away from the octahedral center by about 0.42 Å. The two Cr–N bonds are thus not equivalent in the $CrNCl_2$ monolayer. The optimized lattice constants and bond lengths of $CrNX_2$ (X = Cl, Br, and I) are listed in Table S1.

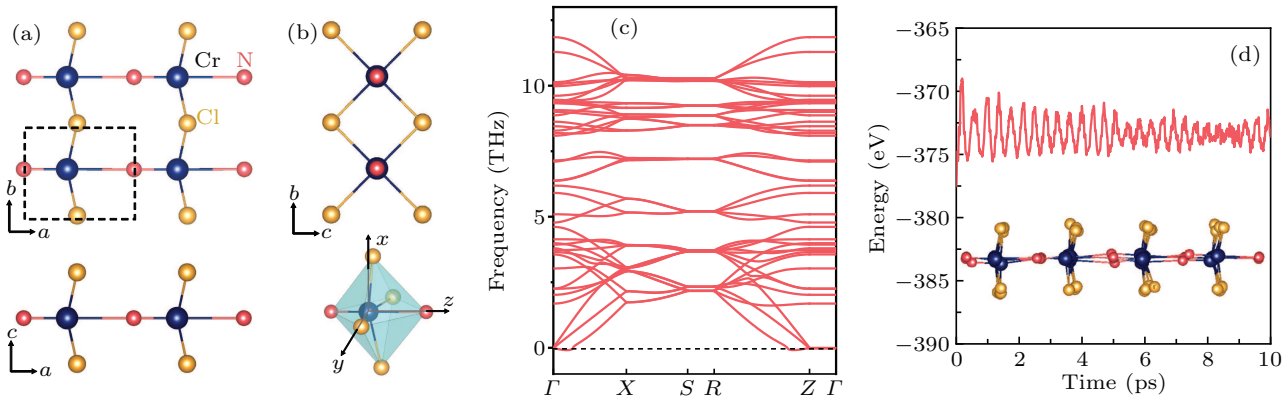


Fig. 1. Crystal structures of the $CrNCl_2$ monolayer: (a) top view along the c axis, side view along the b axis and (b) along the a axis of the supercell. The dashed rectangle indicates the primitive cell. (c) The phonon spectra of the $CrNCl_2$ monolayer. (d) The MD simulations of the $CrNCl_2$ monolayer at a temperature of 500 K for 10 ps. The inset show the side view of the $CrNCl_2$ monolayer at the end of the simulations.

Then the dynamical behavior and thermal stability of the $CrNCl_2$ monolayer are studied. From the phonon spectra in Fig. 1(c), it is found that there are no imaginary-frequency modes, and therefore the $CrNCl_2$ monolayer is dynamically stable. In addition, to verify the thermal stability of the $CrNCl_2$ monolayer, the MD simulations are performed at a temperature of 500 K for 10 ps with a time step of 1.0 fs. As shown in Fig. 1(d), the structure of the $CrNCl_2$ monolayer is presented in this timescale, indicating the thermodynamic stability of the $CrNCl_2$ monolayer at a temperature of up to 500 K. The structural stability of $CrNBr_2$ and $CrNI_2$ monolayers is verified in the supporting information (Figs. S1 and S2).

3.2. Magnetic properties

Here four magnetic configurations (AFM1, AMF2, AFM3 and FM) are considered, as depicted in Figs. 2(a) and 2(b) to find the magnetic ground state (MGS). The results are listed in Table 1. The MGSs of $CrNCl_2$, $CrNBr_2$, and $CrNI_2$ monolayers are AFM1, AFM1 and FM, respectively. The unit cell of the $CrNCl_2$ monolayer is found to be spin-polarized with a total magnetic moment of $\sim 1.0\mu_B$ mainly coming from the d_{xy} orbital of the Cr^{5+} cation, as shown in Fig. 2(c).

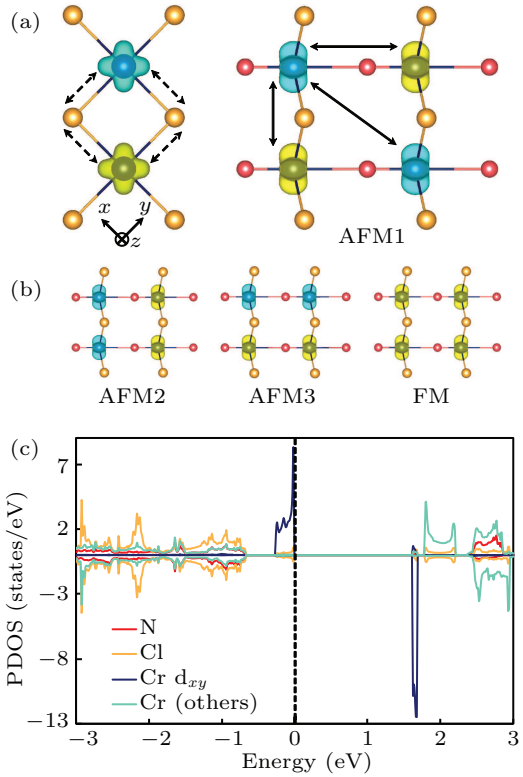


Fig. 2. (a) Top and side views of the spin density isosurfaces of $CrNCl_2$ monolayer with AFM1 order. The solid and dashed arrows refer to the direct d–d exchange and halogen-mediated super exchange, respectively, between the moments on adjacent Cr. (b) Top views of the spin density isosurfaces of $CrNCl_2$ monolayer with AMF2, AFM3 and FM orders. Yellow and blue isosurfaces represent positive and negative spin density, respectively, at the absolute value of 0.3 e/Å^3. (c) Projected density of states (PDOS) of the unit cell in $CrNCl_2$ monolayer with AFM1 order. The valence band maximum is set as zero here.

Table 1. Calculated total energies E (meV) relative to the energy of AFM1 configuration (E_{AFM1}) of four magnetic orders in 2×2 supercells of $CrNCl_2$, $CrNBr_2$ and $CrNI_2$ monolayers.

	E_{AFM1}	E_{AFM2}	E_{AFM3}	E_{FM}	MGS
$CrNCl_2$	0.0	101.6	2.0	91.0	AFM1
$CrNBr_2$	0.0	58.8	2.7	42.3	AFM1
$CrNI_2$	0.0	13.2	6.4	–6.7	FM

In fact, these three monolayers are very similar aside from the radii of different halogen atoms. To further explain their magnetic orders, the magnetic exchange paths along Cr–Cl bond chains (alike for $CrNBr_2$ and $CrNI_2$) are shown in Fig. 2(a). There are two kinds of exchange interactions here. One is direct d–d exchange (shown by solid arrows) between the local moments of adjacent Cr atoms, which will lead to antiparallel spin alignment. The other is the halogen-mediated super exchange (shown by dashed arrows), and it favors a parallel spin alignment according to the Goodenough–Kanamori rule.[43,53] The dominant one of these two interactions will determine the overall magnetic order of the 2D system. It is noteworthy that in systems with larger halogen radius, the physical separation between Cr atoms along b-direction will also be larger, which will weaken the direct exchange. Table 1 shows that for $CrNCl_2$ and $CrNBr_2$, the direct exchange interaction still dominates the magnetic orders at relatively smaller halogen radii, and leads to AFM orders. While in $CrNI_2$, the system shows an FM order with the direct exchange decreasing to be less powerful than the super exchange at such a radius of the halogen I. The weaker direct exchange in $CrNI_2$ is due to the larger b-direction distance than that of $CrNCl_2$ or $CrNBr_2$ (see Table S1). The larger halogen-mediated super exchange in $CrNI_2$ can be explained by the fact that an increased p–d (p orbitals from halogen; d orbitals from Cr) hybridization than that of $CrNCl_2$ or $CrNBr_2$, as shown in Fig. 2(c) and Fig. S4(b). A test on U_{eff} can be found in Table S2.

Monte Carlo simulations on the basis of the 2D Ising Hamiltonian model have been performed to examine the spin dynamics (computational details are shown in the supporting information). The $CrNCl_2$ monolayer has an estimated Néel temperature T_N of 88 K, which is higher than the Curie temperature of 2D $Cr_2Ge_2Te_6$ (20 K),[14] 2D CrI_3 (45 K)[15] and the boiling point of liquid nitrogen (77 K). However, the Néel temperature of $CrNCl_2$ is lower than $VOCl_2$.[41] The Néel temperature of $CrNBr_2$ monolayer is estimated to be 56 K, which is lower than $CrNCl_2$. The Curie temperature of $CrNI_2$ monolayer is estimated to be 38 K. Therefore, the $CrNCl_2$ is more suitable for non-volatile memory devices among the $CrNX_2$ because of its higher Néel temperature.

3.3. Ferroelectric properties

We turn to investigate the intrinsic ferroelectricity of the $CrNCl_2$ monolayer. Usually, a sizable spontaneous polarization is resulted from the breaking of the inversion symmetry in

the $CrNCl_2$ monolayer because of the off-centering displacement of the Cr ion in the octahedron. In the attempt to evaluate the spontaneous polarization, we choose an adiabatic pathway from FE phase, through paraelectric (PE) phase, and to the FE phase with an opposite polarization direction (as the inset of Fig. 3(b)) by using the Berry phase method. The calculations reveal a spontaneous in-plane polarization along the *a*-direction, as shown in Fig. 4(a). In addition, the double well potential of the $CrNCl_2$ monolayer is also depicted in Fig. 4(b) to show the spontaneous polarization along the adiabatic path. The $CrNCl_2$ monolayer is calculated to exhibit a spontaneous polarization of 200 pC/m, which is in the same order of magnitude with those reports of other 2D ferroelectrics (e.g., monolayer group-IV monochalcogenides[28]) and 2D multiferroics (e.g., $VOCl_2$[41]). If the thickness of $CrNCl_2$ monolayer is treated as 1 nm, then the effective polarization in bulk state will be equal to 20.0 μC/cm^2, which is also in the same order of magnitude as those traditional multiferroics materials such as $BiFeO_3$ thin film heterostructures.[54] Therefore, $CrNCl_2$ can be a candidate in logic and memory devices. Also, the calculated spontaneous polarizations of $CrNBr_2$ and $CrNI_2$ are 339 and 310 pC/m, respectively. Furthermore, the total energy of $CrNCl_2$ as a function of spontaneous polarization exhibits a characteristic double-well potential of ferroelectrics, as displayed in Fig. 4(b). The value of the ferroelectric double-well barrier is 1.45 eV/unit-cell, and it is too large for the ferroelectric polarization switching. Therefore, the uniaxial strain is applied on monolayer $CrNCl_2$ in order to reduce the double-well barrier. The calculation results are presented in the supporting information.

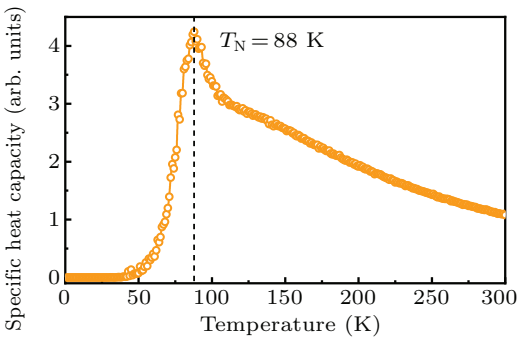


Fig. 3. The specific heat capacity versus temperature for $CrNCl_2$ monolayers, obtained from Monte Carlo simulations on the basis of the 2D Ising Hamiltonian model. Néel temperature is estimated to be 88 K.

The activation barrier reversing in-plane polarization is shown in Fig. 4(c). An intermediate antiferroelectric (AFE) phase is in the middle of the pathway. The energy of AFE phase is 11.3 meV/unit-cell larger than that of FE phase, and the energy barrier between these two phases is as large as 0.68 eV/unit-cell, which makes the FE phase to be robust against thermal fluctuation. This energy barrier of $CrNCl_2$ is much larger than that (0.26 eV) of ferroelectric $LiNbO_3$[55] and that (0.18 eV) of $VOCl_2$,[41] and it indicates that $CrNCl_2$ needs much higher electric field to switch the polarization.

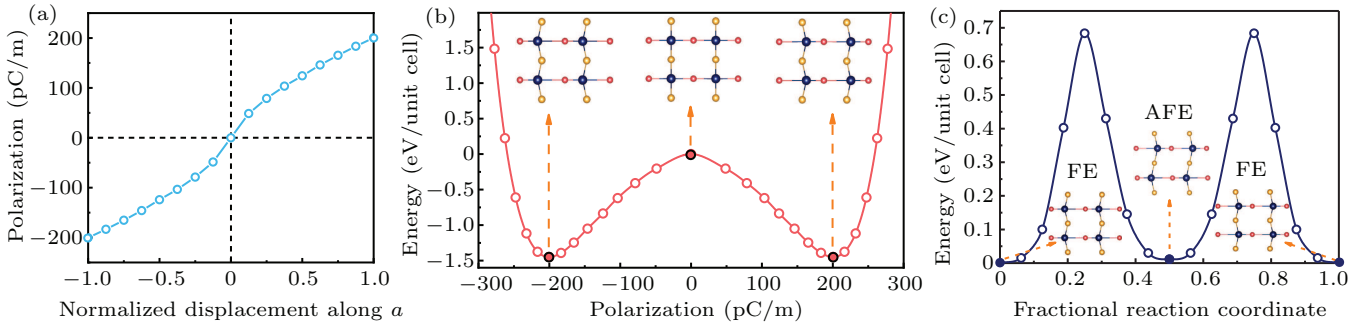


Fig. 4. (a) Total polarization as a function of normalized displacement where the centrosymmetric paraelectric phase (0% displacement) is at the center, and two ferroelectric ground states are at two ends. (b) Doublewell potential of monolayer $CrNCl_2$ along the switching path. (c) Kinetics pathways of the polarization reversal processes in the $CrNCl_2$ monolayer calculated by the CINEB method. The transformation proceeds through a centrosymmetric structure in which the polarization is zero.

The d rule in multiferroic says that generally, the transition metal d electrons have an important role in the occurrence of magnetism.[56] However, those d electrons are believed to suppress the off-center ferroelectric distortion.[56] Then, why would the proposed $CrNCl_2$, $CrNBr_2$ and $CrNI_2$, whose FE characteristics come directly from the Cr^{5+} cation which has a d_{xy} electron, exhibit FM and FE properties at the same time, violating the conventional d^0 rule? As shown in Figs. 2(a) and 2(b), the plane of the d_{xy} orbital of the Cr^{5+} cation is perpendicular to the direction of the FE polarization, which, as a result, hardly suppresses the occurrence of ferroelectricity, and the detailed analysis can be found in the supporting information. This is the similar case with VOX_2 (X = Cl, Br and I). Therefore, the proposed $CrNCl_2$, $CrNBr_2$ and $CrNI_2$ monolayers are calculated to combine the advantages of type-I and type-II multiferroics, showing large polarizations and magnetoelectric coupling. The calculations enrich the search of multiferroics and inspire further research beyond the d rule.

4. Conclusions

In summary, based on first-principles calculations, we have proposed an intrinsic multiferroic, i.e., a $CrNCl_2$ monolayer. It has an antiferromagnetic ground state, with Néel tem-

perature of about 88 K, and it exhibits an in-plane spontaneous polarization of 200 pC/m. The energy barrier reversing polarization is about 0.68 eV/unit-cell, which makes the FE phase to be robust against thermal fluctuation. The d_{xy} orbital of the Cr atom is the origin of magnetic moments but d_{xy} orbital's plane is perpendicular to the direction of the FE polarization, which hardly suppresses the occurrence of ferroelectricity. In addition, like $CrNCl_2$, the $CrNBr_2$ is also an intrinsic multiferroic with antiferromagnetic-ferroelectric ground state while $CrNI_2$ is an intrinsic multiferroic with ferromagnetic-ferroelectric ground states. With the promising properties shown above and in the main text, the $CrNX_2$ multiferroic monolayers show a great potential in applications of nanoscale data storage and spintronics. It is also worth noting that further experimental research is welcomed to build up full and detailed understanding of these 2D multiferroics.

References

[1] Wolf S A, Awschalom D D, Buhrman R A, Daughton J M, von Molnár S, Roukes M L, Chtchelkanova A Y and Treger D M 2001 *Science* **294** 1488
[2] Fert A 2008 *Angew. Chemie Int. Ed.* **47** 5956
[3] Wang X, Du K, Fredrik Liu Y Y, Hu P, Zhang J, Zhang Q, Owen M H S, Lu X, Gan C K, Sengupta P, Kloc C and Xiong Q 2016 *2D Mater.* **3** 031009
[4] Li X and Yang J 2016 *Natl. Sci. Rev.* **3** 365
[5] Novoselov K S, Geim A K, Morozov S V, Jiang D, Zhang Y, Dubonos S V, Grigorieva I V and Firsov A A 2004 *Science* **306** 666
[6] Sun Q, Dai Y, Ma Y, Wei W and Huang B 2015 *RSC Adv.* **5** 33037
[7] Carvalho A, Wang M, Zhu X, Rodin A S, Su H and Castro Neto A H 2016 *Nat. Rev. Mater.* **1** 16061
[8] González-Herrero H, Gómez-Rodríguez J M, Mallet P, Moaied M, Palacios J J, Salgado C, Ugeda M M, Veuillen J Y, Yndurain F and Brihuega I 2016 *Science* **352** 437
[9] Li B, Xing T, Zhong M, Huang L, Lei N, Zhang J, Li J and Wei Z 2017 *Nat. Commun.* **8** 1958
[10] Tong Y, Guo Y, Mu K, Shan H, Dai J, Liu Y, Sun Z, Zhao A, Zeng X C, Wu C and Xie Y 2017 *Adv. Mater.* **29** 1703123
[11] Radhakrishnan S, Das D, Samanta A, de los Reyes C A, Deng L, Alemany L B, Weldeghiorghis T K, Khabashesku V N, Kochat V, Jin Z, Sudeep P M, Martí A A, Chu C W, Roy A, Tiwary C S, Singh A K and Ajayan P M 2017 *Sci. Adv.* **3** e1700842
[12] Zhou Y, Wang Z, Yang P, Zu X, Yang L, Sun X and Gao F 2012 *ACS Nano* **6** 9727
[13] Feng Y P, Shen L, Yang M, Wang A, Zeng M, Wu Q, Chintalapati S and Chang C R 2017 *WIREs Comput. Mol. Sci.* **7** e1313
[14] Gong C, Li L, Li Z, Ji H, Stern A, Xia Y, Cao T, Bao W, Wang C, Wang Y, Qiu Z Q, Cava R J, Louie S G, Xia J and Zhang X 2017 *Nature* **546** 265
[15] Huang B, Clark G, Navarro-Moratalla E, Klein D R, Cheng R, Seyler K L, Zhong D, Schmidgall E, McGuire M A, Cobden D H, Yao W, Xiao D, Jarillo-Herrero P and Xu X 2017 *Nature* **546** 270
[16] Xu Z and Zhu H 2018 *J. Phys. Chem. C* **122** 14918
[17] Wu Q, Zhang Y, Zhou Q, Wang J and Zeng X C 2018 *J. Phys. Chem. Lett.* **9** 4260
[18] Zhu Y, Kong X, Rhone T D and Guo H 2018 *Phys. Rev. Mater.* **2** 081001
[19] Hu T and Kan E J 2018 *Acta Phys. Sin.* **67** 157701 (in Chinese)
[20] Naber R C G, Asadi K, Blom P W M, de Leeuw D M and de Boer B 2010 *Adv. Mater.* **22** 933
[21] Scott J F and Paz de Araujo C A 1989 *Science* **246** 1400
[22] Mathews S, Ramesh R, Venkatesan T and Benedetto J 1997 *Science* **276** 238
[23] Naber R C G, Tanase C, Blom P W M, Gelinck G H, Marsman A W, Touwslager F J, Setayesh S and de Leeuw D M 2005 *Nat. Mater.* **4** 243
[24] Wen Z, Li C, Wu D, Li A and Ming N 2013 *Nat. Mater.* **12** 617
[25] Catalan G and Scott J F 2009 *Adv. Mater.* **21** 2463
[26] Scott J F 2007 *Science* **315** 954
[27] Ahn C H, Rabe K M and Triscone J M 2004 *Science* **303** 488
[28] Fei R, Kang W and Yang L 2016 *Phys. Rev. Lett.* **117** 97601
[29] Fong D D, Stephenson G B, Streiffer S K, Eastman J A, Auciello O, Fuoss P H and Thompson C 2004 *Science* **304** 1650
[30] Junquera J and Ghosez P 2003 *Nature* **422** 506
[31] Shirodkar S N and Waghmare U V 2014 *Phys. Rev. Lett.* **112** 157601
[32] Chang K, Liu J, Lin H, Wang N, Zhao K, Zhang A, Jin F, Zhong Y, Hu X, Duan W, Zhang Q, Fu L, Xue Q K, Chen X and Ji S H 2016 *Science* **353** 274
[33] Liu F, You L, Seyler K L, Li X, Yu P, Lin J, Wang X, Zhou J, Wang H, He H, Pantelides S T, Zhou W, Sharma P, Xu X, Ajayan P M, Wang J and Liu Z 2016 *Nat. Commun.* **7** 12357
[34] Eerenstein W, Mathur N D and Scott J F 2006 *Nature* **442** 759
[35] Cheong S W and Mostovoy M 2007 *Nat. Mater.* **6** 13
[36] Ye Q, Shen Y, Yuan Y, Zhao Y F and Duan C G 2020 *Acta Phys. Sin.* **69** 217710 (in Chinese)
[37] Wang K F, Liu J M and Ren Z F 2009 *Adv. Phys.* **58** 321
[38] Dong S, Liu J M, Cheong S W and Ren Z 2015 *Adv. Phys.* **64** 519
[39] Zhang J J, Lin L, Zhang Y, Wu M, Yakobson B I and Dong S 2018 *J. Am. Chem. Soc.* **140** 9768
[40] Huang C, Du Y, Wu H, Xiang H, Deng K and Kan E 2018 *Phys. Rev. Lett.* **120** 147601
[41] Ai H, Song X, Qi S, Li W and Zhao M 2019 *Nanoscale* **11** 1103
[42] Tan H, Li M, Liu H, Liu Z, Li Y and Duan W 2019 *Phys. Rev. B* **99** 195434
[43] Goodenough J B 1955 *Phys. Rev.* **100** 564
[44] Kresse G and Furthmüller J 1996 *Comput. Mater. Sci.* **6** 15
[45] Kresse G and Furthmüller J 1996 *Phys. Rev. B* **54** 11169
[46] Blöchl P E 1994 *Phys. Rev. B* **50** 17953
[47] Perdew J P, Burke K and Ernzerhof M 1996 *Phys. Rev. Lett.* **77** 3865
[48] Monkhorst H J and Pack J D 1976 *Phys. Rev. B* **13** 5188
[49] Martyna G J, Klein M L and Tuckerman M 1992 *J. Chem. Phys.* **97** 2635
[50] King-Smith R D and Vanderbilt D 1993 *Phys. Rev. B* **47** 1651
[51] Henkelman G, Uberuaga B P and Jónsson H 2000 *J. Chem. Phys.* **113** 9901
[52] Dudarev S L, Botton G A, Savrasov S Y, Humphreys C J and Sutton A P 1998 *Phys. Rev. B* **57** 1505
[53] Goodenough J B 1958 *J. Phys. Chem. Solids* **6** 287
[54] Wang J, Neaton J B, Zheng H, Nagarajan V, Ogale S B, Liu B, Viehland D, Vaithyanathan V, Schlom D G, Waghmare U V, Spaldin N A, Rabe K M, Wuttig M and Ramesh R 2003 *Science* **299** 1719
[55] Singh S, Garcia-Castro A C, Valencia-Jaime I, Muñoz F and Romero A H 2016 *Phys. Rev. B* **94** 161116
[56] Hill N A 2000 *J. Phys. Chem. B* **104** 6694